ANALYSIS OF THE PROJECT
OF INNOVATIVE FLOATING TURBINE

Andrzej Tomporowski[1]
Ali Al-Zubiedy[2]
Józef Flizikowski[1]
Weronika Kruszelnicka[1]
Patrycja Bałdowska-Witos[1]
Jacek Rudnicki[3]

[1] UTP University of Science and Technology, Bydgoszcz, Poland

[2] University of Babylon, Faculty of Materials Engineering, Babylon Hilla, Iraq

[3] Gdańsk University of Technology, Poland

ABSTRACT

The design of a floating, innovative device for river water aeration and conversion of mechanical energy to electrical energy required the analysis of a number of geometrical and dynamic features. Such an analysis may be carried out on the basis of existing methods of numerical fluid mechanics. Models of pressures, forces and torques characteristic for the conversion of watercourse energy were developed for two basic concepts of innovation. These pressures, forces and torques were calculated, designed, and experimentally determined for the variable geometric form and dimensions of the designed working elements of the innovative roller-blade turbine rotor.

Keywords: design, innovative aeration unit, water roller drive

INTRODUCTION

For the need of energy and water aeration on the rivers Tigris (length of 1900 km) and Euphrates (length of 2,700 km) (Turkey, Syria, Iraq), an innovative floating turbine has been designed. 98% of Iraqi water comes from rivers Tigris and Euphrates. The design of the floating device used in the process of river water aeration and conversion of mechanical energy to electricity required the analysis of a number of design features. This analysis may be carried out on the basis of the existing methods of numerical fluid mechanics [1–3].

Despite a relatively simple geometry of the system, the flow in the water wheel area is characterized by considerable complexity. The analysed physical phenomenon is the unsteady two-phase flow [4].

Modelling of flows in rotor machines, with the interaction between rotating and stationary elements, is a known issue [5–9], and a number of models were developed to analyse it. However, the analysis of the water flow in the wheel area requires not only taking into account the movement of the blades, but also their work in different media: water and air, which makes it necessary to apply methods of modelling the interface separation [10, 11].

The complexity of such a model requires time-consuming calculations, including the motion of blades in both media [12–15]. In the light of the identified issues, the specific objectives of the reported research-design work were as follows:

- Developing the model of pressures, forces and torques characteristic for the conversion of watercourse energy, as well as developing the concept of geometric features and parameters of the main working elements of a roll turbine aerator to be used in construction design, manufacturing, and implementation in working components of the innovative power-process unit.
- Experimental recording of pressures, forces and torques in a geometric form having the dimensions of the main working elements of the innovative power-process unit roll turbine aerator.
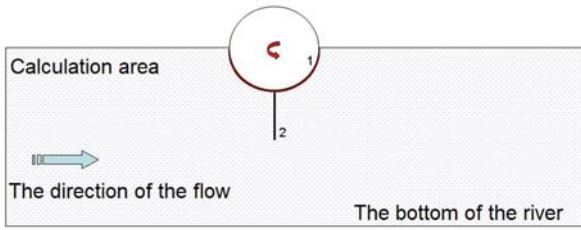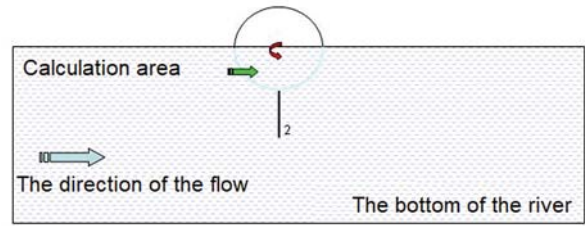
Fig. 1. Calculation area – concept 1A

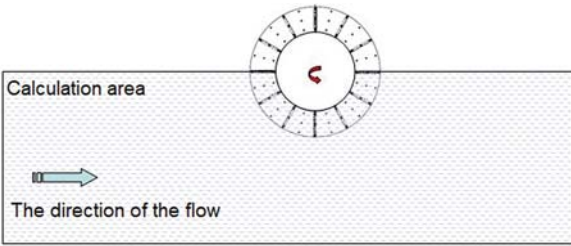Fig. 2. Calculation area – concept 1B
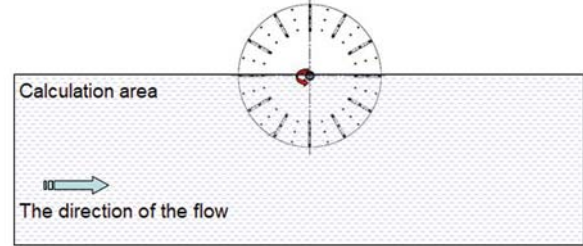

Fig. 3. Calculation area – concept 2A

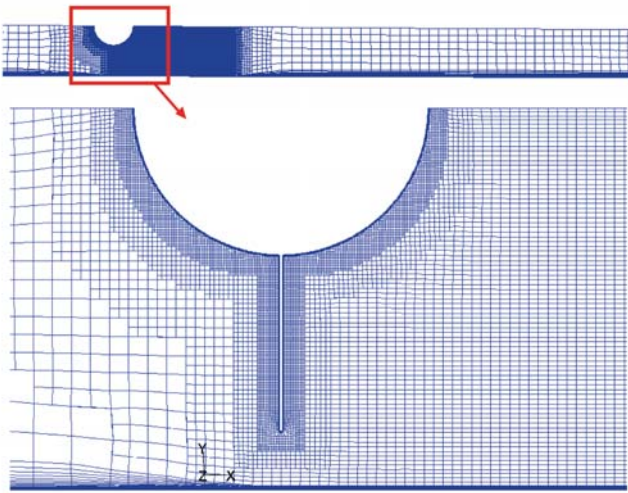Fig. 4. Calculation area – concept 2B

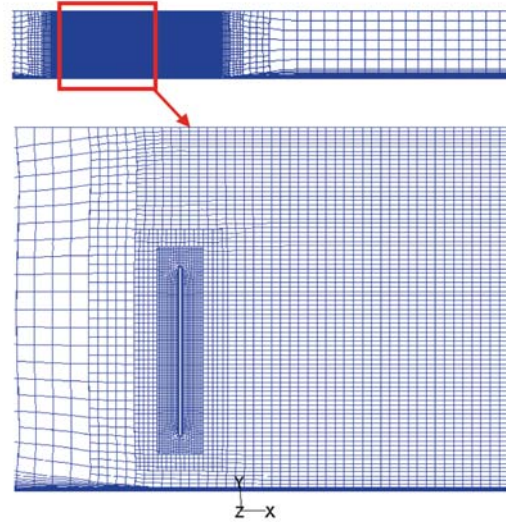Fig. 5. Calculation grid – variant 1A
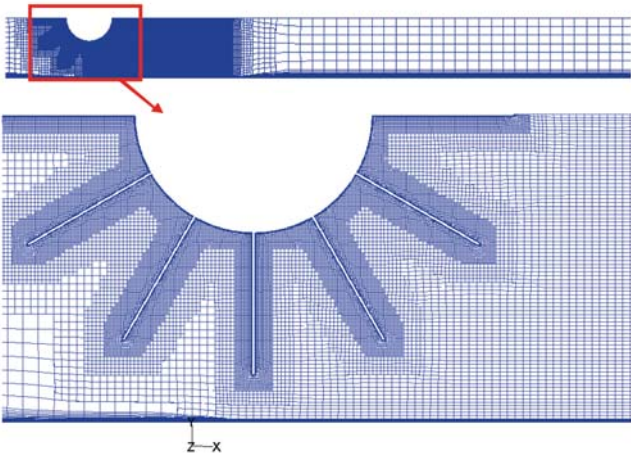

Fig. 6. Calculation grid – variant 1B

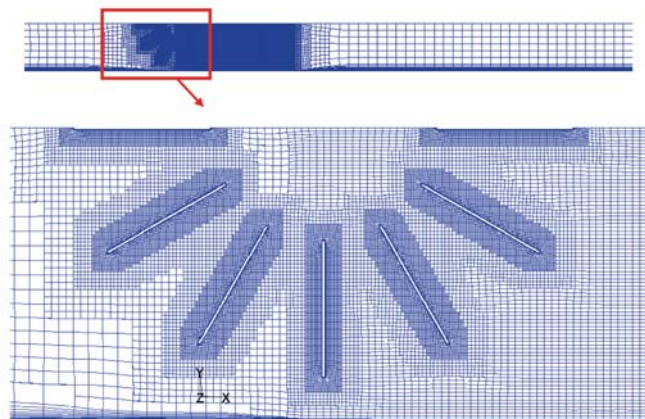Fig. 7. Calculation grid – variant 2A

Fig. 8. Calculation grid – variant 2B

CHARACTERISTICS OF THE CALCULATION MODEL

GEOMETRIC FEATURES OF THE SOLUTION CONCEPTS

The calculations were made for 4 selected concepts of the innovative solution, the configuration of which is shown in Fig. 1 – Fig. 4 [16]. Each figure shows the calculation area with the fragment of the paddle-wheel. Fig. 1 and Fig. 2 show variants 1A and 1B, in which a single blade is mounted in the paddle-wheel. In variant 1A, the blade (2) is seated in the roller (1) being a closed surface, while in variant 1B, the wheel has an openwork structure to allow the medium to flow through it. The geometry shown in variants 2A and 2B (Figures 3 and 4) makes it possible to analyse half of the wheel with all blades installed. Like in variants 1A and 1B, the wheel geometry has the structure with closed surface in variant 2A, and openwork structure in variant 2B. Comparing the calculation results for the above variants enables the evaluation of the performance of a single paddle blade located in the lower position and the effect of its interaction with the neighbouring blades, in terms of forces and moments.

The calculations were performed for the diameter of wheel (1) equal to 1 m and the length of blade (2) equal to 0.6 m. It was assumed that the wheel is half submerged in water. Moreover, 12 blades evenly distributed on the wheel perimeter were assumed in variants 2A and 2B. The calculation grids were made for the two-dimensional flow model. Examples of calculation grids for each variant are presented in Fig. 5 – Fig. 8. In different configurations, a different number of grid elements was generated as a result of the necessity of its sufficient grid thickening in certain perimeter areas. Variants 2A and 2B are characterized by larger number of grid elements than variants 1A and 1B due to the presence of a larger number of blades.

CALCULATION OF FLOW PARAMETERS

The equations used to calculate the flow parameters are the mass conservation equation, Eq. (1), and the momentum conservation equation, Eq. (2) (Table 1). After applying the Newton's hypothesis to the stress tensor, Eq. (3), the momentum conservation equation can be rewritten to the form of Eq. (4). The equations Eq. (1) and Eq. (4) constitute a closed system of 4 scalar equations with 4 unknowns: u_x, u_y, u_z, p, assuming constant density and viscosity of the medium. This equation system allows to obtain a solution taking into account all spatial and temporal scales in the turbulent flow. However, it appears that the minimum number of N grid nodes required to include the vortices at the level of the Kolmogorov scale is proportional to the Reynolds number, Eq. (5), and the number of iterations needed to simulate the flow in a machines rotor (Re$\approx 10^5$) is beyond the capabilities of modern supercomputers.

The analysis of turbulent flows is most often based on the Reynolds hypothesis, according to which the fluid motion is treated as the superposition of the stationary, averaged motion and the unsteady, fluctuating motion.

According to this principle, the value of an arbitrary physical quantity characterising the flow can be presented in the form of Eq. (7). After decomposing the velocity vector u and pressure p into stationary and unsteady parts, and then substituting them to Eq. (7), the Reynolds equation, Eq. (8), is obtained. The Reynolds equation including the mass conservation equation (for incompressible fluid), Eq. (9), is a system of 4 equations with unknowns $\bar{u}_x$, $\bar{u}_y$, $\bar{u}_z$, $\bar{p}$, and the turbulent stress tensor (Reynolds tensor), ρR. This system, Eq. (10), is not closed. Closing the Reynolds equation system requires additional equations determining the components of the turbulence tensor, which is subject to turbulent flow modelling. The method of turbulent flow modelling for which the starting point is the Reynolds equation system belongs to class of RANS (Reynolds Averaged Navier-Stokes) equations, most frequently used in flow analyses. Depending on the formula for the adopted turbulent stress tensor, the following turbulence models can be named [17–20]:

Tab. 1. Calculation of design parameters of flow aerator in turbine

Design characteristics	Model equation	No.
Equation of mass conservation	$\dfrac{\partial \rho}{\partial t} + div(\rho \vec{u}) = 0$	**(1)**
Equation of momentum conservation	$\rho \dfrac{d\vec{u}}{dt} = \rho \vec{f} + divP$	**(2)**
Newton's hypothesis for stress tensor	$P = -(p + \dfrac{2}{3}\mu div\vec{u})E + 2\mu D$	**(3)**
Equation of momentum conservation	$\rho \dfrac{d\vec{u}}{dt} = \rho \vec{f} - gradp + \mu\Delta\vec{u} + \dfrac{1}{3}\mu grad(div\vec{u})$	**(4)**
Minimum number N of calculation grid nodes required to account for vortices at the Kolmogorov scale level – proportional to Reynolds number	$N \sim Re^{9/4}$	**(5)**
Decomposition of arbitrary physical quantity characterizing the flow	$u = \bar{u} + u'$	**(6)**

Design characteristics	Model equation	No.
Equation of momentum conservation (Navier-Stokes) for incompressible fluid	$$\rho\frac{d\vec{u}}{dt} = \rho\vec{f} - gradp + \mu\Delta\vec{u}$$	**(7)**
Reynolds equation after decomposition of velocity vector u and pressure p, and substituting them into Eq. (7)	$$\rho\frac{d\vec{\overline{u}}}{dt} = \rho\vec{f} - grad\overline{p} + \mu\Delta\vec{\overline{u}} - pdivR$$	**(8)**
Mass conservation equation for Reynolds equation (incompressible fluid)	$$div\vec{\overline{u}} = 0$$	**(9)**
System of 4 equations with unknown $\overline{u}_x, \overline{u}_y, \overline{u}_z, \overline{p}$ and turbulent stress tensor (Reynolds tensor) ρR – not closed	$$\rho R = \rho\overline{\vec{u}'\vec{u}'} = \begin{bmatrix} \rho\overline{(u'_x)^2} & \rho\overline{u'_x u'_y} & \rho\overline{u'_x u'_z} \\ \rho\overline{u'_y u'_x} & \rho\overline{(u'_y)^2} & \rho\overline{u'_y u'_z} \\ \rho\overline{u'_z u'_x} & \rho\overline{u'_z u'_y} & \rho\overline{(u'_z)^2} \end{bmatrix}$$	**(10)**
Boussinesq hypothesis based on linear dependence between velocity gradients and Reynolds stress tensor elements	$$R_{ij} = -\frac{2}{3}kE_{ij} + v_t\left(\frac{\partial\overline{u}_i}{\partial x_j} + \frac{\partial\overline{u}_j}{\partial x_i}\right)$$	**(11)**
Transport equation scalar ϕ within single model and two-valued form	$$\frac{\partial\phi}{\partial t} + \overline{u}_i\frac{\partial\phi}{\partial x_i} = \frac{\partial}{\partial x_i}D\frac{\partial\phi}{\partial x_i} + \overset{+}{Z}(\phi) + \overline{Z}(\phi)$$	**(12)**
Transport equations of new variables derived from Navier-Stokes equation	$$\frac{\overline{\partial u'_i u'_j}}{\partial t} + \overline{u}_k\frac{\overline{\partial u'_i u'_j}}{\partial x_k} = P_{ij} + d_{ij} + \Phi_{ij} + \varepsilon_{ij}$$	**(13)**
Kinetic energy of turbulence and specific rate of its dissipation into internal thermal energy	$$\frac{\partial}{\partial t}(\rho k) + \frac{\partial}{\partial x_i}(\rho k u_i) = \frac{\partial}{\partial x_j}\left(\Gamma_k\frac{\partial k}{\partial x_j}\right) + G_k - Y_k$$	**(14)**
	$$\frac{\partial}{\partial t}(\rho\omega) + \frac{\partial}{\partial x_i}(\rho\omega u_i) = \frac{\partial}{\partial x_j}\left(\Gamma_\omega\frac{\partial\omega}{\partial x_j}\right) + G_\omega - Y_\omega + D_\omega$$	**(15)**

1. Models using the concept of turbulent viscosity characterizing the relationship between the turbulence stress tensor and the tensor of medium deformation rate. An example maybe the Boussinesq hypothesis based on linear dependence between the variables, Eq. (11).

Further modelling consists in determining the dependence for turbulent viscosity v_t. For this purpose, additional quantities are introduced to the system of equations, followed by additional equations which allow to determine viscosity and turbulent stresses

The scalar transport equation ϕ within one- and two-equation models takes the form of Eq. (12). On the left-hand side of Eq. (12), there is the evolved substantial derivative, on the right – terms that determine the diffusion coefficient D and positive and negative sources of the given scalar. The equations contain a number of constants, experimentally determined and optimized for several typical flow classes. The turbulence models which are most commonly used now include one-equation models [21] and two-equation models: k-ε [22, 23], RNG k-ε [24], k-ω [25], k-τ [24], k-ω SST [26].

2. Models introducing an additional equation for the Reynolds stress tensor of each component:

    2.1. Algebraic Reynolds stress models (ASM-Algebraic Stress Models), in which the Reynolds stress tensor components are described by algebraic equations, supplemented with the scalar transport equations, e.g. k and ε [27].

    2.1. Models of stress transport (RSM – Reynolds Stress Models), which introduce R_{ij} as new variables, with the equations of their transport derived in the form of Eq. (13) from Navier-Stokes equations.

In these models, individual terms on the right-hand side describe successively production, diffusion, and pressure-velocity correlation of deformation and dissipation. These models require an additional transport equation for ε in order to close the system. Therefore, in the case of three-dimensional flow, additional 7 partial differential equations are added to the system of Reynolds equations [28].

This project uses the two-equation SST k-ω turbulence model. In this model, the kinetic energy of turbulence and the rate of its dissipation are calculated according to Eq. (14) and Eq. (15), where G_k – generation of turbulence kinetic energy; G_ω – characteristics of the intensity of rotary motion; Γ_k – diffusion coefficient of turbulence kinetic energy k; Γ_ω – diffusion coefficient of ω; Y_k – dissipation of k; Y_ω – dissipation of ω; D_ω – term characterizing cross-diffusion.

The system of differential equations describing the fluid motion can be converted to algebraic equations using different

methods [5, 29, 30]. The computational model used in the project is based on the finite volume method. This method uses a form of integral equations of conservation, which is its main characteristic.

The first step of the method is to divide the computational area into sub-areas (control volumes). The calculation points at which the values are unknown functions are placed at the centre of gravity of the control volume. The next step is discretization of partial differential equations, that is, converting them into algebraic equations by integrating after each control volume. The obtained nonlinear algebraic equations are linearized, i.e., nonlinear elements are treated explicitly or implicitly [31–33]. The final stage is interpolation of convective elements and diffusion and source units in the differential schemes. It consists in expressing the average values on the surface of the control volume through the values of the unknown function at the calculated points.

MODEL PARAMETERS
AND BOUNDARY CONDITIONS

The calculations were made using the code Ansys/Fluent 12 and a two-dimensional flow model, assuming its stationarity. The Fluent algorithm is based on the finite volume method, in which transport equations are written in the integral form. The "pressure-based" type solver was used. The convective terms in transport equations were approximated by the 3-rd order MUSCL scheme. The flowing medium was water with constant viscosity of 0.001 kg/m·s, whereas the SST k-ω model was used to describe the turbulent motion.
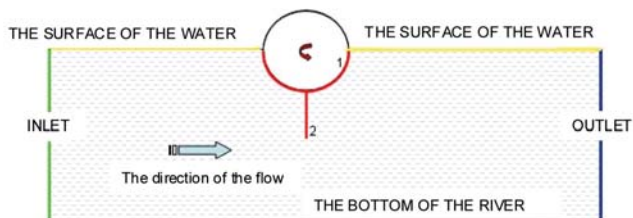

Fig. 9. Scheme of computational area and boundary conditions

The assumed boundary conditions are shown in Fig. 9. At the inlet to the computational area, the "Velocity Inlet" condition was assumed, with the flow velocity value corresponding to the midstream velocity. Additional parameters concerning the turbulence model were the turbulence intensity of 1% and the turbulent-to-laminar viscosity ratio equal to 10. At outlet, the "outflow" condition was assumed. The lower boundary, representing the bottom of the river, was described by the boundary condition "Wall". In contrast, on the free surface, the symmetry condition was assumed, which means that the medium is not transported through this surface, but only slips along it.

Such a set of boundary conditions is a strong simplification of the real situation, especially near the water wheel. However, such an assumption is considered acceptable taking into account the purpose of the analysis, which is to determine forces and moments acting on the blade.

DISCUSSION OF RESULTS

The above presented calculation model was used to determine flow characteristics and forces acting on the blade in the examined variants. Below are given selected results for variants 1A and 2A (full wheel), obtained assuming the flow velocity of 0.1 m·s^{-1} and the depth of 2 m. The latter parameter is the distance of the blade tip from the bottom of the river. Fig. 10 and Fig. 11 show, respectively, pressure and flow velocity distributions, with alluvial power lines for geometry 1A, whereas Fig. 12 – Fig. 14 show the same distributions for geometry 2A. The pressure values are shown as relative values, where the reference pressure is the ambient pressure. The images of flow velocity and power lines indicate high differentiation of the flow structure and velocity values obtained using different calculation models for a single blade and the complete system of blades.
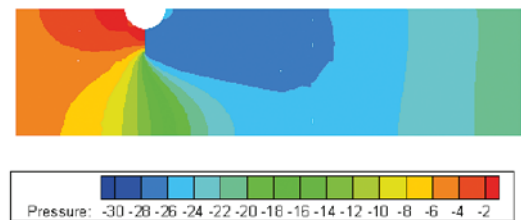

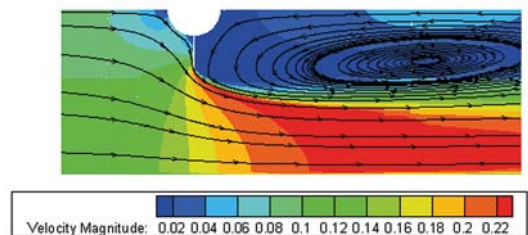Fig. 10. Static pressure – variant 1A
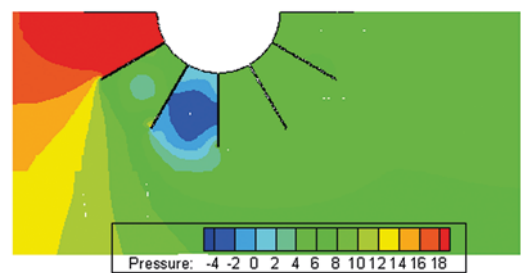

Fig. 11. Velocity and power lines – variant 1A
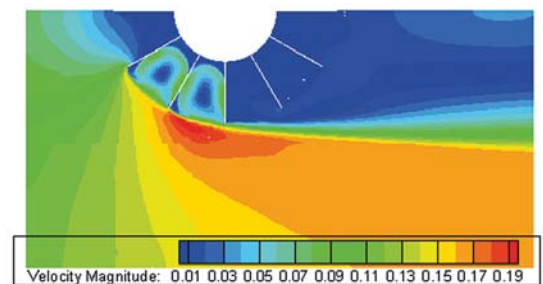

Fig. 12. Static pressure – variant 2A

Fig. 13. Velocity – variant 2A

In each variant, the calculations were performed for 3 flow velocity values: 0.1 m·s⁻¹, 2.7 m·s⁻¹ and 5.5 m·s⁻¹. Moreover, for each case the rotational velocity of the roller blade unit (Fig. 15) was chosen to meet the following condition:

$$u_{lop} \, / \, u = 1 \qquad (16)$$

where:
u – flow velocity,
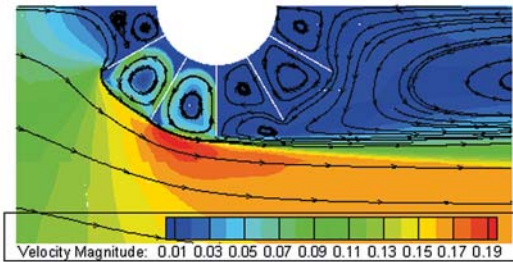u_{lop} – linear velocity of a blade at 2/3 of its length.

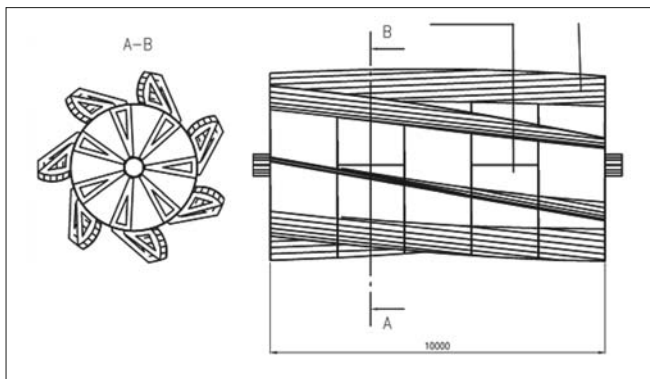Fig. 14. Velocity and power lines – variant 2A

Fig. 15. Turbine roller: constructional form of the cylinder with seven blades (L = 10000 mm)

The resulting rotational speeds of the cylindrical turbine-roller models which met condition (16) for the assumed flow velocities were: 1.06 rpm, 28.6 rpm, and 58.4 rpm. The performed flow calculations allowed to determine the values of moments and forces acting on a single blade or the complete blade system.

In variants 1A and 2A, determining the moment of force is relatively easy and can be obtained from pressure integration over blade surface. These variants are characterized by the existence of a stable solution and stabilized force values in successive steps of the iterative process. Selected time-history of fluctuations of the moment of force recorded during the calculations for variant 1A is shown in Fig. 16. However, determining forces in the presence of unsteady flow in variants 1B and 2B (openwork structure) is more difficult, as it requires unsteady calculations, with further pressure integration not only in space, but also in time. Figs. 17–19 present the time-histories of fluctuations of the moment of force acting on one blade during the calculation process for variant 1B at two different water flow velocities and two water depths. In the case of low flow velocity, the amplitude of fluctuations is relatively small and decreases with increasing depth. On the other hand, when the flow velocity is higher, of 5.5 m·s⁻¹, this amplitude reaches as much as 50% of the average value, which means very large blade load changes and the need to take into account changes in time.

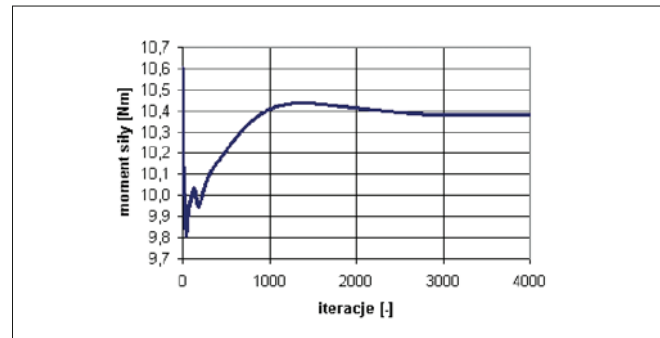

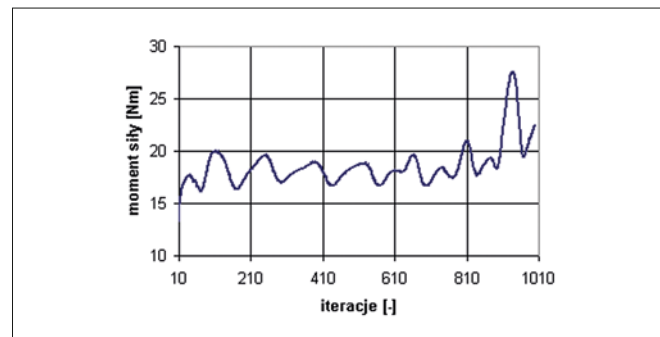Fig. 16. Moment of force acting on the blade: variant 1A, depth 2 m, water flow speed 0.1 m·s⁻¹

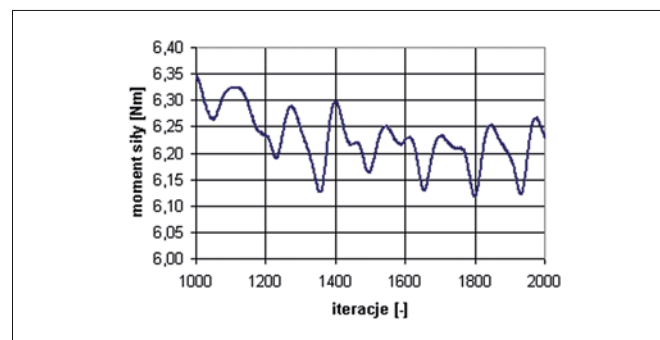Fig. 17. Moment of force acting on the blade: variant 1B, depth 0.2 m, water flow speed 0.1 m·s⁻¹

Fig. 18. Moment of force acing on the blade: variant 1B, depth 2 m, water flow speed 0.1 m·s⁻¹
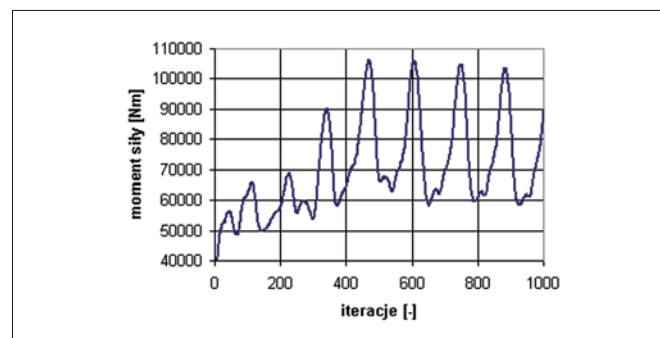
Fig. 19. Moment of force acting on the blade: variant 1B, depth 0.2 m, water flow speed 5.5 m·s⁻¹

Flow velocity		0.1 m·s⁻¹		2.7 m·s⁻¹		5.5 m·s⁻¹	
Rotational speed		1.06 rpm		28.6 rpm		58.4 rpm	
Depth		**0.2 m**	**2 m**	**0.2 m**	**2 m**	**0.2 m**	**2 m**
Variant	1A	252	10	183738	7543	763403	31253
	1B	22.5	6.2	16176	4490	89761	24160
	2A	1.55 95 (1 blade)	0.2 -2.3 (1 blade)	2132 69636 (1 blade)	147 -1704 (1blade)	7416 278940(1 blade)	707 -7227 (1 blade)
	2B	9.5 9 (1 blade)	4.2 -0.6 (1 blade)	10468 6500 (1 blade)	2800 -2000(1 blade)	41000 25000 (1 blade)	3400 -2300 (1 blade)

The exact values of moments of forces recorded for particular variants are collated in Table 2. Each time, the moment of force was determined for the unit width of the blade equal to 1 m. The values marked green in variants 1B and 2B were determined as averages of the calculation process. It should be emphasized again that obtaining accurate values required performing unsteady flow calculations.

A significant difference can be observed between the values of the moment of force acting on the isolated blade and when it is part of the blade system. In variants 2A and 2B, for larger depth G, a negative value of the moment acting on the lower blade was obtained (with a positive torque value for the entire system), which is the effect of the earlier presented pressure distribution.

Larger moment fluctuations are caused by the effect of depth (distance of the blade from the bottom). For a smaller depth, the values are significantly overestimated due to the boundary condition of the non-deformable free surface.

For comparison purposes, Table 3 collates the calculated values of the resistance force and moment acting on a plate having the dimensions of the analysed blade and oriented perpendicular to the flow direction. The force was determined from Eq. (17), where the resistance coefficient c_d was assumed equal to 2 (as appropriate for Reynolds numbers Re>10⁵):

$$F_d = c_d 0.5\rho u^2 A \qquad \textbf{(17)}$$

The moment of force was determined from Eq. (18), assuming that the centre of thrust in this case coincides with the centre of the plate. This configuration is most similar to variant 1B, except the effect of the distance to the bottom and top surfaces of the tank:

$$M_d = F_d(0.5L + R) \qquad \textbf{(18)}$$

Tab. 3. Resistance force and moment acting on flat plate

Flow velocity, m·s⁻¹	0.1	2.7	5.5
Resistance force, N	6	4374	18150
Moment of force, N·m	4.8	3500	14520

There are many solutions, known in the world as small water turbines, which have the form of reaction and reaction turbines, or wastewater, backloading, and backhoe water wheels. The analysed construction of a floating power plant with water turbine consists of a self-supporting, floating roller filled with air. A shaft is placed at the centre of rotation, while coils forming the blades are placed on the circumference of the roller, along the helix. The whole construction is enclosed by a perforated body. The diffuser intensifies taking over the energy from the watercourse. Only some known solutions of the conversion of watercourse energy into the energy of rotational motion were carried out in accordance with the idea of displacement, i.e. the ability to float on the surface or at some favourable depth of the watercourse during energy conversion. In all known solutions, there is a problem with low efficiency [34, 35]. The system collecting the torque from the watercourse is built in such a way that the rotary motion of the positive displacement cylinder is transmitted through the shaft and the mechanical gear to the working unit of the electric power generator. The entire functional system is longitudinally and transversely trapped on the watercourse by blocking it on both sides with anchored ropes. The direction of rotation of the displacement roller with blades results directly from the winding direction of the rotor blades mounted on it. The electric energy generated in the generator is discharged to the users by an electric wire. The water turbine with energy conversion devices, developed according to the presented concept, is characterized by simple and compact structure, which is its unquestionable advantage compared to conventional solutions described, among others, in [36, 37]. The presented structure allowed to eliminate load-bearing units, e.g. as it was used in the solutions presented in [36–38]. The use of a roller with helical blades protects against the destruction of living organisms, including fish, fry, and other aquatic animals. It also generates high torque, according to the Stokes equation, and multiple helices with high coil angle cause low resistance according to Reynolds' dependence, which is an advantage over both the known multi-blade solutions with straight blades, and standard rotors with two and three helical blades [39]. The geometric shape of the working surfaces of the rotor screw coils causes additionally the Magnus effect, which results in the efficiency increase compared to the known solutions of turbines with helical blades [40]. The presented solution may be applied in watercourses as an unconventional

source of renewable energy, especially in places of scarcity and lack of access to the power grid. This device can be used to drive machines and devices without the use of other energy sources, e.g. pumps, and, as a water vehicle propulsion unit, also for educational purposes and popularizing water energy converters.

SUMMARY

For the selected calculation models of the innovative blade-roller unit, models of pressures, forces and torques were developed to model the conversion of watercourse energy in two basic geometrical design concepts and determine new operational parameters of the main elements of the roll turbine aerator. This is important for the needs of detailed pre-implementation design, construction and manufacturing of working elements of the innovative roller-blade unit. The pressures have been determined experimentally, making the basis for calculating forces and torques for a variable geometrical form and dimensions of the projected working elements of the rotor of an innovative roller-blade turbine assembly (for example Fig. 15). In the design concept 1A (Fig. 1), a single blade (2) was mounted on a roller (1) being a closed surface, while in variant 2A (Fig. 3), the wheel had an openwork structure to allow the medium to flow through it. Determining the moment of force was relatively easy for these two cases and was obtained from pressure integration over blade surfaces. These variants are characterized by the existence of a stable solution and stabilized force values in successive steps of the iterative process. For the selected design concepts, forces and moments were determined for individual configurations in assumed flow conditions, which was the preparation stage for implementation of the roller-blade assembly in the conditions of the Tigris and Euphrates rivers. The obtained results of calculations will enable determination of the flow through the structure and the assessment of its effect on the system of forces in the roller blade. These results were used for initial assessment of basic construction parameters, being the starting point to further more advanced calculations using complex physical models. The calculations were made for the concept of a full roll (roll surface) and open-work structure (without a roll). In both cases the analysis was carried out for a single blade and the complete blade system, assuming two channel depths and 3 watercourse speeds. The results of the calculations lead to the following specific conclusions:

1. The calculation model of two-dimensional, stationary and single-phase flow with the assumption of a non-deformable free surface well reflects the reality only in variants 1A and 2A, provided that the channel has a sufficiently large depth, i.e. the distance of the lower blade tip from the bottom.
2. In variants 1B and 2B, the flow past blades from the side of the lower and top channels causes the formation of the flow structure which requires the use of a non-stationary flow model.
3. The determined forces and moments indicate the significant effect of the depth of the channel on the obtained results. The moment of force increases with decreasing depth.
4. The structure of the flow indicates the need to analyse the entire blade system to determine forces acting on it. The analysis of a single blade can be useful in the design and evaluation of its float. But the difference in the structure of flow and the recorded force values between the simplified configuration and the full blade system will grow with the increase of blade length and the decrease of channel depth. These values can differ by one or, for small depths, two orders of magnitude, which makes the single-blade calculation results useless for design purposes.
5. The analysis of the designed flows, leading to a quantitative assessment of the effect of construction parameters of the floating power roll and aeration, requires time-consuming calculations with the unsteady two-phase model taking into account the motion of roll elements.
6. In variants 1A and 2A, the use of an innovative hydroelectric turbine with the aeration option refers to watercourse conditions with a sufficiently large channel depth, i.e. the distance of the lower blade tip from the bottom.
   The determined forces and moments indicate a clear influence of channel depth on the obtained values. The torque increases with decreasing depth.
7. The flow structure indicates the need for extending the calculation and for devising drum solutions with a single, preferably oblique, canopy forming the roll/drum.

REFERENCES

1. Basumatary, M., Biswas, A., Misra, R.D.: *CFD analysis of an innovative combined lift and drag (CLD) based modified Savonius water turbine*. Energy Convers. Manag. 174, 72–87 (2018). https://doi.org/10.1016/j.enconman.2018.08.025.

2. Sritram, P., Suntivarakorn, R.: *Comparative Study of Small Hydropower Turbine Efficiency at Low Head Water*. Energy Procedia. 138, 646–650 (2017). https://doi.org/10.1016/j.egypro.2017.10.181.

3. Jiyun, D., Hongxing, Y., Zhicheng, S., Xiaodong, G.: *Development of an inline vertical cross-flow turbine for hydropower harvesting in urban water supply pipes*. Renew. Energy. 127, 386–397 (2018). https://doi.org/10.1016/j.renene.2018.04.070.

4. Viollet, P.-L.: *From the water wheel to turbines and hydroelectricity. Technological evolution and revolutions*. Comptes Rendus Mécanique. 345, 570–580 (2017). https://doi.org/10.1016/j.crme.2017.05.016.

5. Ferziger, J.H., Perić, M.: *Computational methods for fluid dynamics*. Springer, Berlin; New York (2002).

6. Flizikowski, J., Topoliński, T., Opielak, M., Tomporowski, A., Mroziński, A.: *Research and analysis of operating characteristics of energetic biomass mikronizer*. Eksploat. Niezawodn. 17, 19–26 (2015).

7. Tomporowski, A., Flizikowski, J.: *Motion characteristics of a multi-disc grinder of biomass grain*. Przem. Chem. 92, 498–503 (2013).

8. Flizikowski, J.B., Kruszelnicka, W., Tomporowski, A., Mrozinski, A.: *A study of operating parameters of a roller mill with a new design*. AIP Conf. Proc. 2077, 020018 (2019). https://doi.org/10.1063/1.5091879.

9. Tomporowski, A., Flizikowski, J, Kruszelnicka, W.: *A new concept of roller-plate mills*. Przem. Chem. 96, 1750–1755 (2017). https://doi.org/10.15199/62.2017.8.29.

10. Du, J., Shen, Z., Yang, H.: *Effects of different block designs on the performance of inline cross-flow turbines in urban water mains*. Appl. Energy. 228, 97–107 (2018). https://doi.org/10.1016/j.apenergy.2018.06.079.

11. Jiyun, D., Zhicheng, S., Hongxing, Y.: *Performance enhancement of an inline cross-flow hydro turbine for power supply to water leakage monitoring system*. Energy Procedia. 145, 363–367 (2018). https://doi.org/10.1016/j.egypro.2018.04.065.

12. Kruszelnicka, W., Flizikowski, J., Tomporowski, A.: *Auto-monitoring system of grainy biomass comminution technology*. IOP Conf. Ser. Mater. Sci. Eng. 393, 012076 (2018). https://doi.org/10.1088/1757-899X/393/1/012076.

13. Tongphong, W., Saimek, S.: *The Design and Development of an Oscillating Water Turbine*. Energy Procedia. 52, 552–558 (2014). https://doi.org/10.1016/j.egypro.2014.07.109.

14. Wang, J., Piechna, J., Müller, N.: *A novel design of composite water turbine using CFD*. J. Hydrodyn. Ser B. 24, 11–16 (2012). https://doi.org/10.1016/S1001-6058(11)60213-8.

15. Tomporowski, A., Flizikowski, J., Kasner, R., Kruszelnicka, W.: *Environmental Control of Wind Power Technology*. Rocz. Ochr. Śr. 19, 694–714 (2017).

16. Flaszyński, P.: *Wyniki obliczeń przepływowych w następstwie obliczenia sił i momentów obrotowych uzyskiwanych dla założonych parametrów konstrukcyjnych projektowanej turbiny*, (2011).

17. Boxma, O., Zwart, B.: *Fluid flow models in performance analysis*. Comput. Commun. 131, 22–25 (2018). https://doi.org/10.1016/j.comcom.2018.07.009.

18. Tang, M., Yuan, L., He, S., Fu, T.: *Simplified modeling of YPL fluid flow through a concentric elliptical annular pipe*. J. Pet. Sci. Eng. 162, 225–232 (2018). https://doi.org/10.1016/j.petrol.2017.12.030.

19. Sondermann, C.N., Baptista, R.M., Bastos de Freitas Rachid, F., Bodstein, G.C.R.: *Numerical simulation of non-isothermal two-phase flow in pipelines using a two-fluid model*. J. Pet. Sci. Eng. 173, 298–314 (2019). https://doi.org/10.1016/j.petrol.2018.10.018.

20. Rasti, E., Talebi, F., Mazaheri, K.: *A turbulent duct flow investigation of drag-reducing viscoelastic FENE-P fluids based on different low-Reynolds-number models*. Phys. Stat. Mech. Its Appl. (2019). https://doi.org/10.1016/j.physa.2019.03.083.

21. Spalart, P., Allmaras, S.: *A one-equation turbulence model for aerodynamic flows*. In: 30th Aerospace Sciences Meeting and Exhibit. American Institute of Aeronautics and Astronautics (1992). https://doi.org/10.2514/6.1992-439.

22. Launder, B., Spalding, D.B.: *Mathematical Models of Turbulence*. Academic Press, London (1972).

23. Launder, B.E., Sharma, B.I.: *Application of the energy-dissipation model of turbulence to the calculation of flow near a spinning disc*. Lett. Heat Mass Transf. 1, 131–137 (1974).

24. Yakhot, V., Orszag, S.A., Thangam, S., Gatski, T.B., Speziale, C.G.: *Development of turbulence models for shear flows by a double expansion technique*. Phys. Fluids Fluid Dyn. 4, 1510–1520 (1992). https://doi.org/10.1063/1.858424.

25. Wilcox, D.C.: *Turbulence Modeling for CFD*. D C W Industries, La Cãnada, Calif (2006).

26. Menter, F.R.: *Two-equation eddy-viscosity turbulence models for engineering applications*. AIAA J. 32, 1598–1605 (1994). https://doi.org/10.2514/3.12149.

27. Launder, B.E., Reece, G.J., Rodi, W.: *Progress in the development of a Reynolds-stress turbulence closure*. J. Fluid Mech. 68, 537–566 (1975). https://doi.org/10.1017/S0022112075001814.

28. Gavrilov, A.A., Rudyak, V.Y.: *Reynolds-averaged modeling of turbulent flows of power-law fluids*. J. Non-Newton. Fluid Mech. 227, 45–55 (2016). https://doi.org/10.1016/j.jnnfm.2015.11.006.

29. Fletcher, C.A.J.: *Computational Techniques for Fluid Dynamics*, Vol. 1: Fundamental and General Techniques. Springer-Verlag, NY (1991).

30. Hirsch, C.: *Numerical Computation of Internal and External Flows: The Fundamentals of Computational Fluid Dynamics – 2nd Edition*. Elsevier (2007).

31. Tomporowski, A., Flizikowski, J., Wełnowski, J., Najzarek, Z., Topoliński, T., Kruszelnicka, W., Piasecka, I., Śmigiel, S.: *Regeneration of rubber waste using an intelligent grinding system*. Przem. Chem. 97, 1659–1665 (2018). https://doi.org/10.15199/62.2018.10.6.

32. Rudnicki, J., Zadrag, R.: *Technical State Assessment of Charge Exchange System of Self-Ignition Engine, Based on the Exhaust Gas Composition Testing*. Pol. Marit. Res. 24, 203–212 (2017). https://doi.org/10.1515/pomr-2017-0040.

33. Korczewski, Z., Rudnicki, J.: *An Energy Approach to the Fatigue Life of Ship Propulsion Systems Marine 2015*. In: Salvatore, F., Broglia, R., and Muscari, R. (eds.) VI International Conference on Computational Methods in Marine Engineering – The Conference Proceedings. pp. 490–501. Int Center Numerical Methods Engineering, 08034 Barcelona (2015).

34. Flizikowski, J.: *Apparatus for aerating water courses and disintegrating solid impurities contained in their water,* http://regserv.uprp.pl/register/application?number=P.308679, (1999).

35. Green Tech Avenue: *Micro Hydro Power Technology – 5kW WATER TURBINE*, https://translate.google.com/translate?hl=pl&sl=en&u=http://www.greentechavenue.com/wp-content/uploads/2011/Greentechavenue_micro_hydro_power_solution.pdf&prev=search.

36. Matulewicz, W.: *Floating water – power plant*. Przegląd Elektrotechniczny. 1, 279–283 (2015). https://doi.org/10.15199/48.2015.09.68.

37. Dąbała, K., Krzemień, Z., Olszewski, A.: *Micro hydropower station with a spiral turbine*. Zesz. Probl. – Masz. Elektr. 129–133 (2009).

38. Rangan, P.R., Karnyoto, A.S., Ambabunga, Y.A.M., Rambulangi, A.C.: *Design of River Flow Floating Portable Micro-Hydro*. Int. J. Eng. Tech. 4, 593–597 (2018).

39. Nguyen, M.H., Jeong, H., Yang, C.: *A study on flow fields and performance of water wheel turbine using experimental and numerical analyses*. Sci. China Technol. Sci. 61, 464–474 (2018). https://doi.org/10.1007/s11431-017-9146-9.

40. Akimoto, H., Tanaka, K., Uzawa, K.: *A conceptual study of floating axis water current turbine for low-cost energy capturing from river, tide and ocean currents*. Renew. Energy. 57, 283–288 (2013). https://doi.org/10.1016/j.renene.2013.02.002.

CONTACT WITH THE AUTHORS

Andrzej Tomporowski
e-mail: a.tomporowski1@wp.pl

UTP University of Science and Technology
Al. S. Kaliskiego 7, 85-796 Bydgoszcz
Poland

Ali Al-Zubiedy
e-mail: mat.ali.alzubiedy@oubabylon.edu.iq

University of Babylon, Faculty of Materials Engineering,
Najaf Road, 14km from the center of Hilla,
P.O. Box 4 Babylon Hilla
Iraq

Józef Flizikowski
e-mail: fliz@utp.edu.pl

UTP University of Science and Technology
Al. S. Kaliskiego 7, 85-796 Bydgoszcz
Poland

Weronika Kruszelnicka
e-mail: weronika.kruszelnicka@utp.edu.pl

UTP University of Science and Technology
Al. S. Kaliskiego 7, 85-796 Bydgoszcz
Poland

Patrycja Bałdowska-Witos
e-mail: patrycja.baldowska-witos@utp.edu.pl

UTP University of Science and Technology
Al. S. Kaliskiego 7, 85-796 Bydgoszcz
Poland

Jacek Rudnicki
e-mail: jacekrud@pg.edu.pl

Gdańsk University of Technology
Narutowicza 11/12, 80-233 Gdańsk
Poland